IEEE Access
Multidisciplinary ⋮ Rapid Review ⋮ Open Access Journal

Received 3 January 2024, accepted 12 January 2024, date of publication 6 February 2024, date of current version 14 February 2024.

Digital Object Identifier 10.1109/ACCESS.2024.3362876

RESEARCH ARTICLE

Multi-Element Self-Decoupled MIMO Patch Antenna With Flexible Characteristics

HUNG TRAN-HUY[1], HONG NGUYEN TUAN[2], NGUYEN QUOC DINH[3], DUC-NGUYEN TRAN-VIET[4], AND HYUN-CHANG PARK[5], (Member, IEEE)

[1]Faculty of Electrical and Electronic Engineering, Phenikaa University, Hanoi 12116, Vietnam
[2]Center for High Technology Development, Vietnam Academy of Science and Technology (VAST), Hanoi 10000, Vietnam
[3]Advanced Wireless Communications Group, Le Quy Don Technical University, Hanoi 11917, Vietnam
[4]Faculty of Radio-Electronic Engineering, Le Quy Don Technical University, Hanoi 11917, Vietnam
[5]Division of Electronics and Electrical Engineering, Dongguk University, Seoul 04620, South Korea

Corresponding author: Hyun-Chang Park (hcpark@dongguk.edu)

This work was supported in part by the Dongguk University Research Fund of 2023, and in part by the Vietnam Academy of Science and Technology (VAST) under Grant TĐANQP.02/23–25.

ABSTRACT This paper presents a multi-element multiple-input multiple-output (MIMO) antenna with self-isolation and flexible characteristics. The primary radiators of the proposed antenna consist of multiple ellipse-shaped patches arranged in an H-plane configuration. Self-decoupling is achieved by simultaneously different operating modes on the excited element (TM_{10} mode) and non-excited element (TM_{02} mode). The proposed method also shows strong extensibility. The measurements on the fabricated 4-element MIMO antenna demonstrate that the proposed decoupling method can improve the isolation by 14 dB. The antenna shows good MIMO diversity performances with respect to the envelope correlation coefficient and diversity gain. Additionally, the antenna also works effectively in when the substrate is bent, which contributes to significantly increasing the applicability of the proposed method in comparison with the other reported methods.

INDEX TERMS MIMO antenna, self-decoupled, patch, multi-element.

I. INTRODUCTION

In the era of fifth-generation (5G) mobile networks with the rapid development of multi-antenna systems, Multiple Input Multiple Output (MIMO) antennas have attracted significant attention due to their potential to improve wireless communication efficiency and channel capacity. However, optimizing the separation between MIMO antenna elements has many challenges, as their high mutual coupling significantly degrades radiation performances.

Numerous solutions have been proposed to reduce coupling between antenna elements. The first method, known as the suppression scheme, has been extensively studied with a focus on suppressing coupling effects through the utilization of defective ground structures (DGS) [1], [2], [3], metamaterials [4], [5], and resonators [6], [7], [8]. However, it is worth noting that the use of DGS structures can lead to an increase in backward radiation, and metamaterial structures may not be suitable for contemporary compact device designs due to their bulky structure.

The second type of decoupling method is the counteraction scheme. Additional coupling paths are introduced to counteract the original coupling. The well-known configurations include decoupling networks [9], [10], [11], neutralization lines [12], [13], [14], or parasitic elements [15], [16], [17], [18]. Despite achieving high isolation, additional decoupling structures considerably increase the complexity and dimensions of the MIMO system.

The third decoupling method to overcome the deficiencies of the above-mentioned methods is self-isolation. The primary advantage of this approach is its ability to improve antenna isolation based on the intrinsic characteristics of the antenna itself, eliminating the need for additional decoupling networks. Several representative works have been presented [19], [20], [21], [22], [23], [24], [25]. In [19], the mutual coupling is mitigated by adjusting the feeding

The associate editor coordinating the review of this manuscript and approving it for publication was Stefan Schwarz.

position. Another method is to use a special ground design with slots [20]. In [21] and [22], the patch is cut with various shapes of slots. In [23], the self-decoupling technique is based on the weak field on the patch. Another decoupling scheme using mode-counteraction is presented in [25]. Although high isolation can be achieved, such MIMO antennas work effectively only in the normal mode due to their lack of flexibility features. Additionally, the method proposed in [19], [20], [21], [22], [23], [24], and [25] cannot be extended to multi-element MIMO arrays.

This paper introduces a self-decoupling technique to suppress mutual coupling between microstrip patch MIMO antennas. The proposed method can be applied to a two-element H-plane coupled MIMO antenna and can be scaled up to a multi-element antenna array while maintaining excellent isolation. Moreover, another advantage of the utilized self-decoupling method is its flexibility, which has not been addressed in the previous studies. A thorough literature review reveals that there are several flexible MIMO antennas using microstrip structures [26], [27], [28], [29]. Nonetheless, these designs suffer from high profiles and large element spacings [27], [28]. Additionally, the extension to multiple elements has not been discussed in such designs.

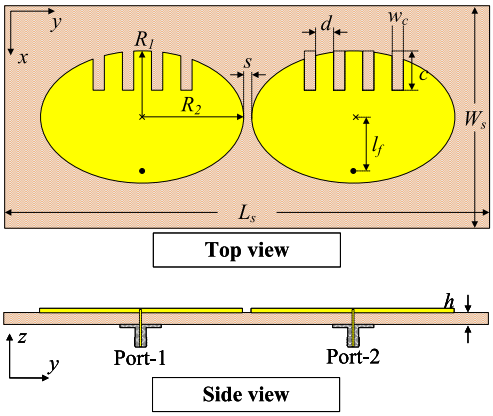

FIGURE 1. Geometry of the proposed 2-element MIMO antenna.

II. TWO-ELEMENT MIMO ANTENNA

A. ANTENNA OPERATION

Fig. 1 shows the geometry of the proposed 2-element self-decoupled MIMO antenna with respect to the top view and cross-section view. Two ellipse-shaped patches are arranged in the H-plane coupling configuration. The antenna is printed on both sides of a ROGER-5880 substrate with a dielectric constant of 2.2. Two 50-Ω SMA connectors are used to excite the antenna. The optimized parameters are as follows: $L_s = 90$, $W_s = 40$, $h = 0.5$, $R_1 = 11.8$, $R_2 = 18$, $l_f = 8.4$, $s = 1$, $l_c = 7$, $w_c = 2$, $d = 2.5$ (unit: mm).

The simulated scattering parameter (S-parameter) results of the self-decoupled and coupled MIMO antennas are illustrated in Fig. 2. Note that both antennas are optimized so that they have similar operating frequencies and the element-spacing is fixed for both cases. The simulated results indicate that the isolation of the self-decoupled

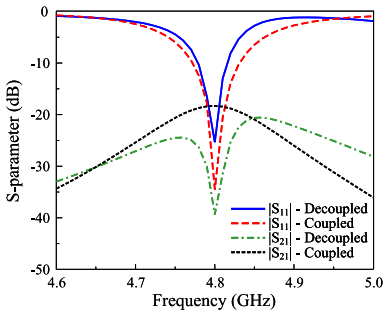

FIGURE 2. Simulated S-parameter of the self-decoupled and coupled MIMO antennas.

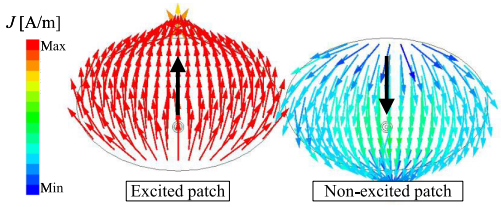

FIGURE 3. Current distribution of the coupled MIMO antenna.

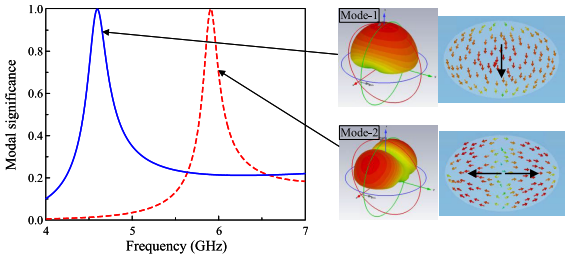

FIGURE 4. CMA on the ellipse-shaped patch with $R_1 = 11.8$ mm and $R_2 = 18.0$ mm.

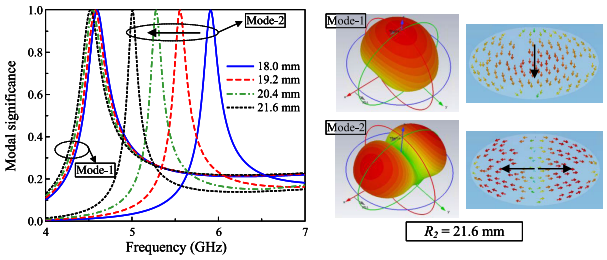

FIGURE 5. CMA on the ellipse-patched with different values of major radius, R_2.

MIMO antenna is significantly higher than the coupled MIMO, which is 18 dB compared to 39 dB. The isolation improvement is about 21 dB at the resonant frequency of 4.8 GHz.

B. DECOUPLING MECHANISM

The current distribution on the coupled MIMO antenna is first investigated for a better understanding of the decoupling mechanism. Fig. 3 shows the vector surface current at the resonant frequency of 4.8 GHz. It can be seen that the induced current on the non-excited element has a similar direction to the current on the excited patch. Here, both are working in the fundamental mode of TM_{10}, leading to high mutual coupling.

To suppress the mutual coupling without using any additional decoupling structure, a possible solution is to change the operating mode on the non-excited element, while keeping the fundamental mode on the excited element. The operating modes on a single ellipse-shaped patch antenna can be revealed by using The Characteristic Mode Analysis (CMA) [30]. According to the CMA, the modal significance is used to identify the possible radiation of an arbitrary mode. The characteristic modes could be obtained by solving the equations below [31]:

$$\vec{J} = \sum_n a_n J_n \tag{1}$$

where a_n and J_n are the modal weighting coefficient and the eigencurrent, respectively.

$$a_n = \frac{V_n^i}{1 + j\lambda_n} \tag{2}$$

Here, V_n^i is the modal excitation coefficient, while λ_n is the eigenvalue. The normalized amplitude of the current modes represents the modal significance, MS_n, which can be determined by the following equation [31]:

$$MS_n = \left| \frac{1}{1 + j\lambda_n} \right| \tag{3}$$

When the modal significance is close to 1, it indicates the resonant capability of the mode. Fig. 4 shows the CMA on the proposed patch antenna in the frequency range from 4 to 7 GHz. It can be seen obviously that there are two dominant modes around 4.6 and 5.9 GHz. Based on the current distributions, these modes are respectively the fundamental mode (TM_{10}) and the higher-order mode (TM_{02}). Next, Fig. 5 shows the CMA when increasing the major axis of the ellipse patch. As observed, the higher-order mode shifts towards the lower frequencies of 5.6 and 5.0 GHz with $R_2 = 19.2$ and 21.6 mm. The current distributions of Mode-1 and Mode-2 with $R_2 = 21.6$ mm are consistent with the fundamental TM_{10} and high-order TM_{02} modes shown in Fig. 4.

Based on the above-mentioned study, the self-isolation scheme is to produce the fundamental TM_{10} mode on the excited patch, while the other operates in the higher TM_{02} mode. When these modes have similar operating frequencies, high isolation can be obtained. According to the CMA, this requirement can be achieved by tuning the major axis of the ellipse-shaped patch while fixing the minor axis. However, increasing the major axis leads to a large antenna geometry. Thus, the meander-line structure is embedded into the patch, as shown in Fig. 1. The meander-line structure helps to increase the electrical length of the TM_{02} mode without causing any significant effect on the TM_{10} mode. Fig. 6 shows the current distribution at 4.8 GHz of the MIMO antenna with the meander-line structure. The distribution behavior is almost similar to that of the TM_{02} mode depicted in Fig. 4, which demonstrates the design concept.

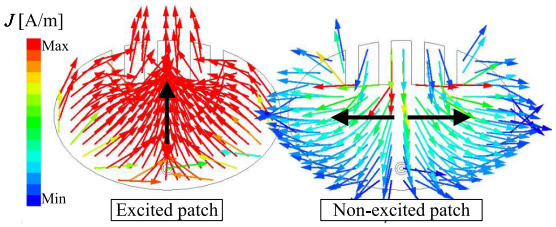

FIGURE 6. Current distribution on the ellipse-shaped patch with meander-line structure.

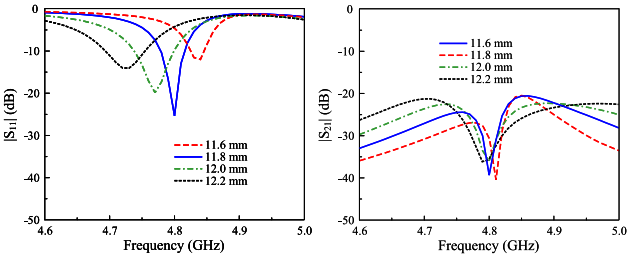

FIGURE 7. Simulated S-parameter for different values of R_1.

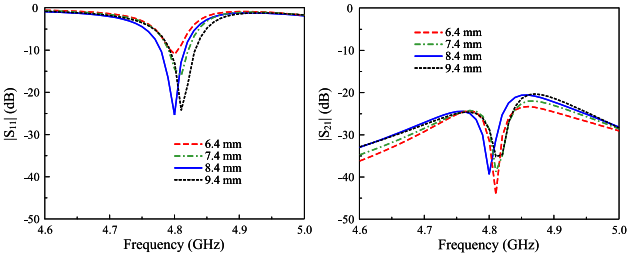

FIGURE 8. Simulated S-parameter for different values of l_f.

C. ANTENNA OPTIMIZATION PROCESS

The optimization process of the proposed antenna can be achieved after implementing several key parameter studies. Firstly, Fig. 7 shows the simulated reflection coefficient and transmission coefficient for different values of R_1. It can be seen that tuning this parameter has a strong effect on the $|S_{11}|$ resonance, which shifts downwards with increasing R_1. Meanwhile, the effect on the isolation feature is minor. The dip in the $|S_{21}|$ profile is quite stable.

Secondly, the antenna performance for different feeding positions is studied. The simulated S-parameter against the variation of l_f is depicted in Fig. 8. As observed, the resonant frequencies in the $|S_{11}|$ and $|S_{21}|$ profiles are stable. Meanwhile, the matching is considerably affected by different values of l_f. With l_f = 8.4 mm, the optimized reflection coefficient value at 4.8 GHz is achieved.

Finally, the isolation is significantly affected by the length (l_c) and width (w_c) of the slot. In general, the movement of the dip in the $|S_{21}|$ profile is more significant than that in the $|S_{11}|$ profile when tuning these parameters. As seen in Fig. 9, increasing l_c leads to lower dips in both $|S_{11}|$ and $|S_{21}|$ profiles. Regarding w_c, when the slot becomes narrower, its effect on the total length along the major axis is minor. Thus, the isolation with w_c = 1.6 mm shows a

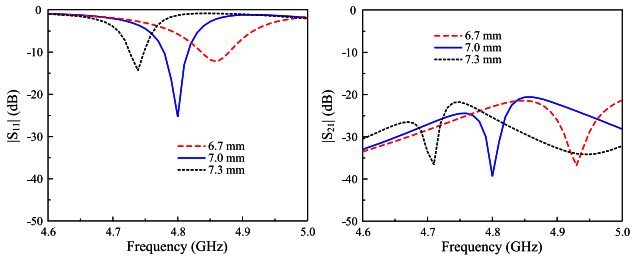

FIGURE 9. Simulated S-parameter for different values of l_c.

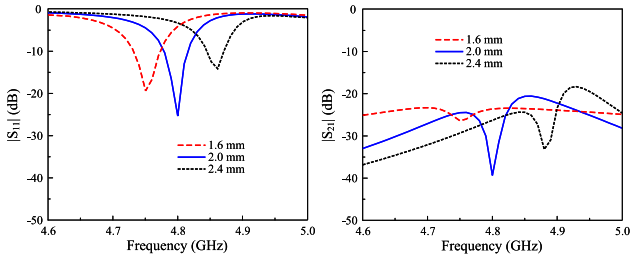

FIGURE 10. Simulated S-parameter for different values of w_c.

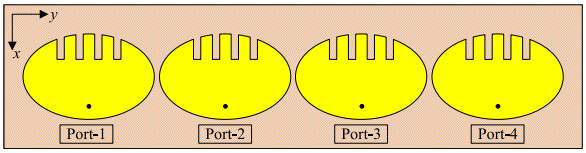

FIGURE 11. Geometry of the proposed 4-element MIMO array.

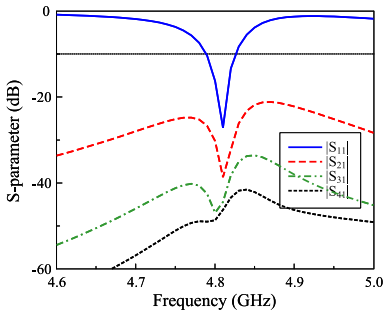

FIGURE 12. Simulated S-parameter of the 4-element MIMO array.

small improvement in comparison with the coupled MIMO (presented in Fig. 2). According to this study, it can be concluded that the dimensions of the slot play an important role in determining the isolation performance at the desired operating frequency.

III. FOUR-ELEMENT MIMO ANTENNA

A. ANTENNA DESIGN

The proposed self-isolation scheme is also extendable to multi-element MIMO arrays. For demonstration, Fig. 11 shows the geometry of a four-element patch array. It is worth noting that in this design, the element spacing and the dimensions of the patches are kept the same as the above-mentioned 1×2 MIMO array. This demonstrates the scalability of the proposed self-decoupling technique. The overall dimensions of the antenna are 160 mm $\times$ 40 mm.

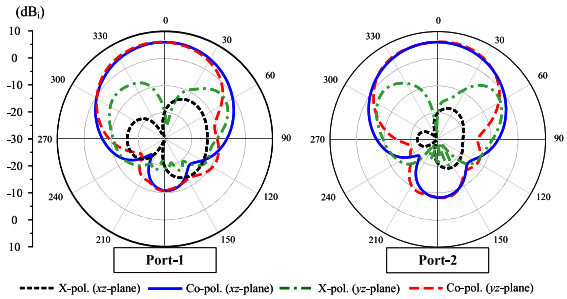

FIGURE 13. Simulated gain radiation patterns at 4.75 GHz with different port excitations.

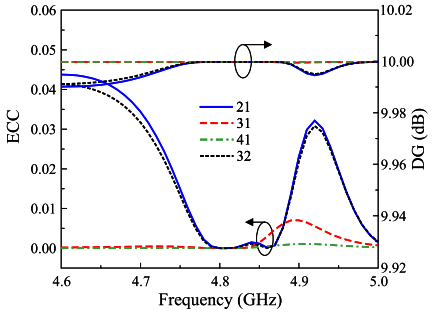

FIGURE 14. Calculated ECC and DG of the proposed 4-element MIMO array.

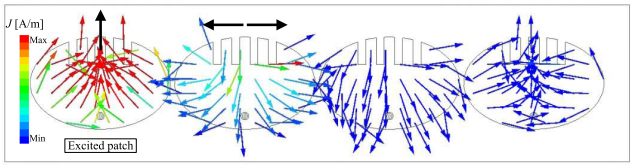

FIGURE 15. Current distribution on the proposed MIMO array.

B. ANTENNA CHARACTERISTIC

Fig. 12 shows the S-parameters of the proposed self-decoupled 4-element MIMO antenna array. As seen, the self-decoupled MIMO performs a high inter-port isolation value of better than 30 dB. The radiation patterns at the center operating frequency with Port-1 and Port-2 excitations are plotted in Fig. 13. Obviously, the patterns are almost similar for both excited ports. The antenna exhibits a good radiation pattern, which is quite symmetric around the broadside direction. The broadside gain is about 6.0 dBi. The difference between the co- and cross-polarization in the broadside direction is very high, which is better than 25 dB. Besides, the front-to-back ratio is higher than 15 dB.

The MIMO diversity performances in terms of envelop correlation coefficient (ECC) and diversity gain (DG) are presented in Fig. 14. They are calculated based on the S-parameter, which has been thoroughly discussed in [32]. The acceptable value of ECC is lower than 0.5, and the DG is approximately 10 dB. As seen, the calculated ECC values are much smaller than 0.5. Meanwhile, the DG values are close to the maximum value of 10 dB.

Finally, the current distribution at 4.8 GHz of the proposed 4-element MIMO array is shown in Fig. 15. It is seen that the

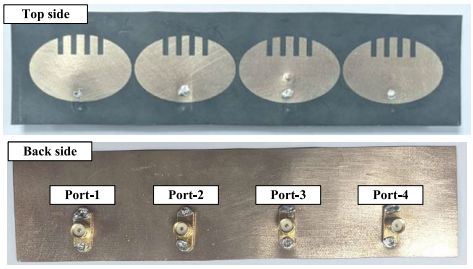

FIGURE 16. Photographs of the fabricated 1 × 4 MIMO antenna array.

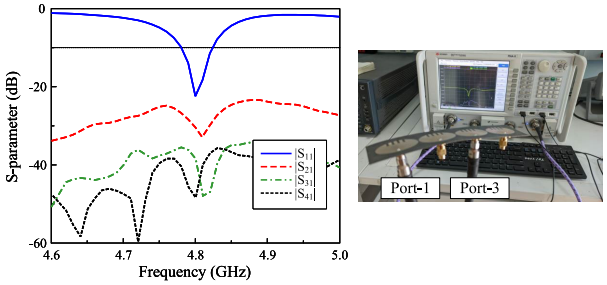

FIGURE 17. Measured S-parameter of the fabricated 1 × 4 MIMO antenna array in normal mode.

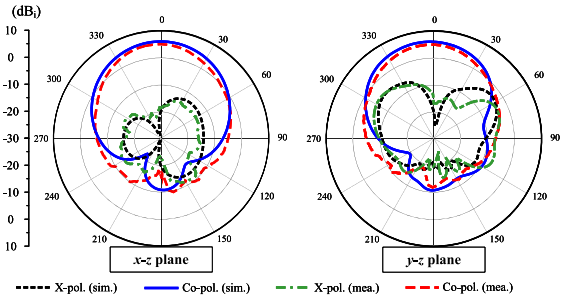

FIGURE 18. Measured radiation patterns of the proposed 1 × 4 MIMO antenna array.

mode on the excited patch is the fundamental mode, while the others are in orthogonal higher-order mode. This is consistent with the operation of the 2-element MIMO antenna discussed in Section II.

IV. DESIGN PROCEDURE

Based on the parameter studies in Section II and the design of the four-element MIMO antenna, the optimization process for a 1 × N MIMO array can be summarized as follows:

- Step 0: Design the ellipse-shaped patch with the feeding position on the minor axis.
  - The length of the minor axis is about a half-effective-wavelength at the desired frequency band, resulting in the fundamental TM_{10} mode.
  - Along the major axis, the meander-line structure is added. The whole length in the major axis is about one effective wavelength at the desired frequency to make sure that the TM_{02} mode is similar to the TM_{10} mode.

TABLE 1. Performance comparison among MIMO antennas using microstrip structure.

Ref.	Decoupling method	Antenna profile (λ)	Edge spacing (λ)	Operating BW (%)	Isolation (dB)	Flexi-bility	Extensi-bility
[8]	Near-field resonators	0.05	0.04	6	>20	No	Yes
[15]	Parasitic elements	0.09	0.05	14.8	>20	No	Yes
[20]	Self-decoupling	0.04	0.02	6.7	>10	No	Yes
[21]	Self-decoupling	0.04	0.14	2.9	>20	No	Yes
[23]	Self-decoupling	0.04	0.18	3.4	>10	No	Yes
[25]	Self-decoupling	0.03	0.12	1.8	>20	No	Yes
[26]	Self-decoupling	0.02	0.24	4.9	>30	Yes	No
[27]	Polarization diversity	0.04	0.18	3.4	>20	Yes	Yes
[28]	Electromagnetic bandgap	0.03	0.08	<3.0	>20	Yes	No
[29]	Self-decoupling	0.02	0.09	27.6	>34	Yes	No
Prop.	Self-decoupling	0.01	0.03	<3.0	>26	Yes	Yes

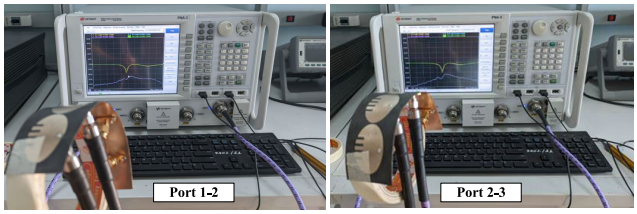

FIGURE 19. Measurement setup in flexible mode.

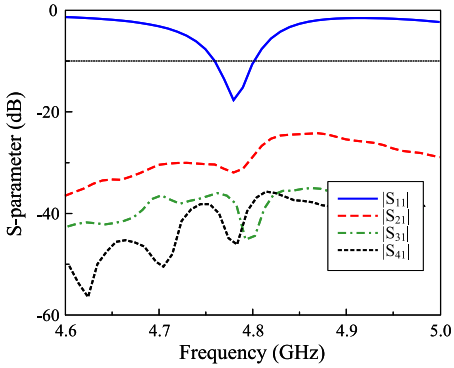

FIGURE 20. Measured S-parameter of the fabricated 1 × 4 MIMO antenna array in flexible mode.

- Step 1: Tune the meander line structure including (l_c, w_c, d) so that the 2-element MIMO antenna has the best isolation at the desired frequency.
- Step 2: Tune the minor axis (R_1) so that the dip in the $|S_{11}|$ profile of the 2-element MIMO antenna is similar to the dip in the $|S_{21}|$ profile.
- Step 3: Optimize the feeding position (l_f) for the best matching performance.
- Step 4: Final-tune all design parameters.
- Step 5: Design the 1 × N MIMO array by increasing the number of ellipse-shaped patches in the H-plane.

V. MEASUREMENT

Fig. 16 presents the photographs of the top side and bottom side of the fabricated four-element MIMO array. The prototype is measured using a vector network analyzer for S-parameter check and an anechoic chamber for far-field radiation features. When comparing the simulations and measurements, there is a minor difference attributed to the tolerances in manufacturing and measurement.

A. NORMAL MODE

The measured S-parameter results of the fabricated prototype are illustrated in Fig. 17. As seen, the measured −10 dB impedance is from 4.78 to 4.82 GHz. Across this band, the measured inter-ports isolation is always better than 26 dB. The maximum isolation is observed at 4.8 GHz, which is better than 32 dB.

The far-field radiation patterns at 4.8 GHz with Port-1 excitation are plotted in Fig. 18. Note that due to the symmetric configuration and the high self-isolation feature, the results for the other port excitations are similar to Port-1 excitation. It can be seen that in both principal planes of E- and H-plane, the antenna exhibits well-measured radiation patterns. The measured broadside gain is about 5.4 dBi. The polarization discrimination in the broadside direction is 18 dB. Meanwhile, the front-to-back ratio is about 15 dB. These measured values are close to the simulated values presented in Section III.

B. FLEXIBLE MODE

As demonstrated in Section IV, the proposed MIMO antenna is also expected to work effectively in flexible scenarios. Here, due to the flexibility of the utilized ROGER-5880 substrate, the antenna can bend to the radius of 50 mm while having a good S-parameter around 4.8 GHz. Figs. 19 and 20 present the measured S-parameter of the antenna with R_{bend} = 50 mm. The measured data demonstrate that the antenna exhibits good operation characteristics. The matching performance and the isolation are fairly maintained around 4.8 GHz. Note that with higher values of R_{bend}, the results become more similar to those of the unbent case. Accordingly, the proposed MIMO array works effectively in flexible mode.

VI. COMPARISON WITH RELATED WORKS

The comprehensive comparison among microstrip patch MIMO antenna arrays is summarized and given in Table 1. Although the designs [8], [15], [21], [23], [27], and [28] can achieve wideband operation, they suffer from large edge-to-edge spacings of greater than 0.04 λ and low inter-port isolation, which is better than 20 dB across the operating BW. In comparison with the self-decoupled MIMO antennas in [21] and [23], the proposed self-decoupling method achieves much smaller spacing while having higher isolation. Additionally, it can work in flexible mode. Compared with the flexible MIMO arrays [27] and [28] the proposed array has smaller element spacing and the capability to extend to a larger scale 1-dimensional MIMO array.

VII. CONCLUSION

This paper has presented and investigated the multi-element MIMO array with flexible characteristics. The self-decoupling method is used to decouple multiple H-plane coupled ellipse-shaped patches. By exciting the fundamental mode TM_{10} and higher-order mode TM_{02} on the excited and non-excited elements, respectively at the same time, high isolation can be achieved without using any additional external circuit. The measurements have been carried out to demonstrate the feasibility of the proposed concept. The antenna shows good matching, isolation, as well as MIMO diversity performances. It is also worth noting that the proposed self-decoupling method can work effectively in flexible mode.

REFERENCES

[1] C. Caloz, H. Okabe, T. Iwai, and T. Itoh, "A simple and accurate model for microstrip structures with slotted ground plane," *IEEE Microw. Wireless Compon. Lett.*, vol. 14, no. 4, pp. 133–135, Apr. 2004.

[2] F. Zhu, J. Xu, and Q. Xu, "Reduction of mutual coupling between closely-packed antenna elements using defected ground structure," in *Proc. 3rd IEEE Int. Symp. Microw., Antenna, Propag. EMC Technol. Wireless Commun.*, 2009, pp. 1–4.

[3] M. M. Bait-Suwailam, O. F. Siddiqui, and O. M. Ramahi, "Mutual coupling reduction between microstrip patch antennas using slotted-complementary split-ring resonators," *IEEE Antennas Wireless Propag. Lett.*, vol. 9, pp. 876–878, 2010.

[4] S. Luo, Y. Li, Y. Xia, and L. Zhang, "A low mutual coupling antenna array with gain enhancement using metamaterial loading and neutralization line structure," *Appl. Comput. Electromagn. Soc. J. (ACES)*, vol. 34, no. 3, pp. 411–418, 2019.

[5] R. Mark, N. Rajak, K. Mandal, and S. Das, "Metamaterial based superstrate towards the isolation and gain enhancement of MIMO antenna for WLAN application," *AEU Int. J. Electron. Commun.*, vol. 100, pp. 144–152, Feb. 2019.

[6] M.-C. Tang, X. Chen, T. Shi, H. Tu, Z. Wu, and R. W. Ziolkowski, "A compact, low-profile, broadside radiating two-element Huygens dipole array facilitated by a custom-designed decoupling element," *IEEE Trans. Antennas Propag.*, vol. 69, no. 8, pp. 4546–4557, Aug. 2021.

[7] R. Karimian, A. Kesavan, M. Nedil, and T. A. Denidni, "Low-mutual-coupling 60-GHz MIMO antenna system with frequency selective surface wall," *IEEE Antennas Wireless Propag. Lett.*, vol. 16, pp. 373–376, 2017.

[8] M. Li, B. G. Zhong, and S. W. Cheung, "Isolation enhancement for MIMO patch antennas using near-field resonators as coupling-mode transducers," *IEEE Trans. Antennas Propag.*, vol. 67, no. 2, pp. 755–764, Feb. 2019.

[9] Y.-M. Zhang, Q.-C. Ye, G. F. Pedersen, and S. Zhang, "A simple decoupling network with filtering response for patch antenna arrays," *IEEE Trans. Antennas Propag.*, vol. 69, no. 11, pp. 7427–7439, Nov. 2021.

[10] B. C. Pan and T. J. Cui, "Broadband decoupling network for dual-band microstrip patch antennas," *IEEE Trans. Antennas Propag.*, vol. 65, no. 10, pp. 5595–5598, Oct. 2017.

[11] M. Li, L. Jiang, and K. L. Yeung, "A novel wideband decoupling network for two antennas based on the Wilkinson power divider," *IEEE Trans. Antennas Propag.*, vol. 68, no. 7, pp. 5082–5094, Jul. 2020.

[12] C.-X. Mao, S. S. Gao, Y. Wang, and J. T. S. Sumantyo, "Compact broadband dual-sense circularly polarized microstrip antenna/array with enhanced isolation," *IEEE Trans. Antennas Propag.*, vol. 65, no. 12, pp. 7073–7082, Dec. 2017.

[13] S. Su, C. Lee, and F.-S. Chang, "Printed MIMO-antenna system using neutralization-line technique for wireless USB-dongle applications," *IEEE Trans. Antennas Propag.*, vol. 60, no. 2, pp. 456–463, Feb. 2012.

[14] C.-D. Xue, X. Y. Zhang, Y. F. Cao, Z. Hou, and C. F. Ding, "MIMO antenna using hybrid electric and magnetic coupling for isolation enhancement," *IEEE Trans. Antennas Propag.*, vol. 65, no. 10, pp. 5162–5170, Oct. 2017.

[15] H. H. Tran and N. Nguyen-Trong, "Performance enhancement of MIMO patch antenna using parasitic elements," *IEEE Access*, vol. 9, pp. 30011–30016, 2021.

[16] M. A. Sufian, N. Hussain, A. Abbas, J. Lee, S. G. Park, and N. Kim, "Mutual coupling reduction of a circularly polarized MIMO antenna using parasitic elements and DGS for V2X communications," *IEEE Access*, vol. 10, pp. 56388–56400, 2022.

[17] K. D. Xu, J. Zhu, S. Liao, and Q. Xue, "Wideband patch antenna using multiple parasitic patches and its array application with mutual coupling reduction," *IEEE Access*, vol. 6, pp. 42497–42506, 2018.

[18] M. Li and S. Cheung, "Isolation enhancement for MIMO dielectric resonator antennas using dielectric superstrate," *IEEE Trans. Antennas Propag.*, vol. 69, no. 7, pp. 4154–4159, Jul. 2021.
[19] Y. He, Y.-F. Cheng, and J. Luo, "Self-decoupled MIMO antenna realized by adjusting the feeding positions," *Electronics*, vol. 11, no. 23, p. 4004, Dec. 2022.
[20] Q. X. Lai, Y. M. Pan, and S. Y. Zheng, "A self-decoupling method for MIMO antenna array using characteristic mode of ground plane," *IEEE Trans. Antennas Propag.*, vol. 71, no. 3, pp. 2126–2135, Mar. 2023.
[21] Q. X. Lai, Y. M. Pan, S. Y. Zheng, and W. J. Yang, "Mutual coupling reduction in MIMO microstrip patch array using TM10 and TM02 modes," *IEEE Trans. Antennas Propag.*, vol. 69, no. 11, pp. 7562–7571, Nov. 2021.
[22] O. Sokunbi, H. Attia, A. Hamza, A. Shamim, Y. Yu, and A. A. Kishk, "New self-isolated wideband MIMO antenna system for 5G mm-wave applications using slot characteristics," *IEEE Open J. Antennas Propag.*, vol. 4, pp. 81–90, 2023.
[23] H. Lin, Q. Chen, Y. Ji, X. Yang, J. Wang, and L. Ge, "Weak-field-based self-decoupling patch antennas," *IEEE Trans. Antennas Propag.*, vol. 68, no. 6, pp. 4208–4217, Jun. 2020.
[24] Q. Li, Y. Wei, M. Tan, X. Lei, G. Wu, M. Huang, and Y. Gong, "Flexibly extensible planar self-isolated wideband MIMO antenna for 5G communications," *Electronics*, vol. 8, no. 9, p. 994, Sep. 2019.
[25] Q. X. Lai, Y. M. Pan, and S. Y. Zheng, "Mode-counteraction based self-decoupling in circularly polarized MIMO microstrip patch array," *IEEE Trans. Antennas Propag.*, vol. 70, no. 10, pp. 9337–9346, Oct. 2022.
[26] L. Yang, Y. Xie, H. Jia, M. Qu, Z. Lu, and Y. Li, "Dual-band flexible MIMO antenna with self-isolation enhancement structure for wearable applications," *Chin. J. Electron.*, vol. 32, no. 4, pp. 692–702, Jul. 2023.
[27] S. Yan, P. J. Soh, and G. A. E. Vandenbosch, "Dual-band textile MIMO antenna based on substrate-integrated waveguide (SIW) technology," *IEEE Trans. Antennas Propag.*, vol. 63, no. 11, pp. 4640–4647, Nov. 2015.
[28] A. A. Althuwayb, M. Alibakhshikenari, B. S. Virdee, N. Rashid, K. Kaaniche, A. B. Atitallah, A. Armghan, O. I. Elhamrawy, C. H. See, and F. Falcone, "Metasurface-inspired flexible wearable MIMO antenna array for wireless body area network applications and biomedical telemetry devices," *IEEE Access*, vol. 11, pp. 1039–1056, 2023.
[29] D. Wen, Y. Hao, M. O. Munoz, H. Wang, and H. Zhou, "A compact and low-profile MIMO antenna using a miniature circular high-impedance surface for wearable applications," *IEEE Trans. Antennas Propag.*, vol. 66, no. 1, pp. 96–104, Jan. 2018.
[30] Y. Chen and C.-F. Wang, *Characteristic Modes: Theory and Applications*. Hoboken, NJ, USA: Wiley, 2015.
[31] R. Harrington and J. Mautz, "Theory of characteristic modes for conducting bodies," *IEEE Trans. Antennas Propag.*, vol. AP-19, no. 5, pp. 622–628, Sep. 1971.
[32] A. Abbas, N. Hussain, M. A. Sufian, W. A. Awan, J. Jung, S. M. Lee, and N. Kim, "Highly selective multiple-notched UWB-MIMO antenna with low correlation using an innovative parasitic decoupling structure," *Eng. Sci. Technol., Int. J.*, vol. 43, Jul. 2023, Art. no. 101440.

HUNG TRAN-HUY received the B.S. degree in electronics and telecommunications from the Hanoi University of Science and Technology, Hanoi, Vietnam, in 2013, the M.S. degree in electrical engineering from Ajou University, in 2015, and the Ph.D. degree in electrical engineering from Dongguk University, South Korea, in 2020. He is currently a Lecturer with the Department of Electrical and Electronic Engineering, Phenikaa University, Hanoi, Vietnam. His research interests include polarized antennas, MIMO antennas, metamaterial-based antennas, and reconfigurable antennas.

HONG NGUYEN TUAN received the Ph.D. degree in applied physics from Ajou University, South Korea, in 2010. He is currently a Scientist with the Center for High Technology Development (HTD), Vietnam Academy of Science and Technology. His current research interests include space instrumentation, carbon-based nanomaterials, and nanocomposites.

NGUYEN QUOC DINH received the B.E., M.E., and D.E. degrees from the Department of Electrical and Electronic Engineering, National Defense Academy, Yokosuka, Japan, in 2006, 2008, and 2011, respectively. Since 2011, he has been a Research Associate with the Faculty of Radio-Electronics Engineering, Le Quy Don Technical University. He is currently an Associate Professor with the Advanced Wireless Communications Group, Le Quy Don Technical University, Hanoi, Vietnam. His research interests include very small antennas, array antennas, UWB antennas, and MIMO antennas. He is a member of the Institute of Electronics, Information and Communication Engineers (IEICE), Japan. He was a recipient of the Young Scientist Award from the IEICE Antennas and Propagation Society Japan Chapter, Japan, in 2011.

DUC-NGUYEN TRAN-VIET received the B.S. degree in communication command from Telecommunications University, Vietnam, in 2011, and the M.S. degree in electronics engineering from Le Quy Don Technical University, Hanoi, Vietnam, in 2017, where he is currently pursuing the Ph.D. degree. His research interests include circularly polarized antennas, MIMO antennas, and metamaterial-based antennas.

HYUN-CHANG PARK (Member, IEEE) received the B.S. degree in electronics engineering from Seoul National University, Seoul, South Korea, in 1986, and the M.S. and Ph.D. degrees in electrical engineering from Cornell University, Ithaca, NY, USA, in 1989 and 1993, respectively.

From 1993 to 1995, he was a Research Associate with the Department of Electrical Engineering, University of Virginia, Charlottesville, VA, USA. In 1995, he joined the Department of Electronics and Electrical Engineering, Dongguk University, Seoul, South Korea, where he is currently a Professor. His research interests include RF energy harvesting, wideband/multi-band planar antennas, and reconfigurable antennas for various wireless applications.